ACS APPLIED MATERIALS & INTERFACES

Research Article

Cite This: ACS Appl. Mater. Interfaces 2019, 11, 28851−28857

www.acsami.org

Impurity Tracking Enables Enhanced Control and Reproducibility of Hybrid Perovskite Vapor Deposition

Juliane Borchert,[†] Ievgen Levchuk,[‡,§] Lavina C. Snoek,[†] Mathias Uller Rothmann,[†] Renée Haver,[∥] Henry J. Snaith,[†] Christoph J. Brabec,[‡,⊥] Laura M. Herz,[†] and Michael B. Johnston*,[†]

[†]Department of Physics, University of Oxford, Clarendon Laboratory, Parks Road, Oxford OX1 3PU, United Kingdom

[‡]Materials for Electronics and Energy Technology (i-MEET), Friedrich-Alexander-Universität Erlangen-Nürnberg, Martensstraße 7, 91058 Erlangen, Germany

[§]Energy Campus Nürnberg (EnCN), Fürther Str. 250, 90429 Nürnberg, Germany

[∥]Department of Chemistry, Chemistry Research Laboratory, University of Oxford, OX1 3TA Oxford, United Kingdom

[⊥]FZ Jülich, HI-ErN (IEK-11), Erlangen, Immerwahrstrasse 2, D-91058 Erlangen, Germany

Supporting Information

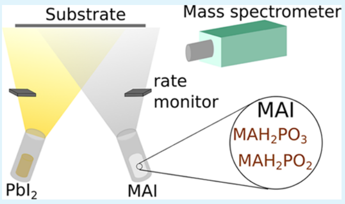

ABSTRACT: Metal halide perovskite semiconductors have the potential to enable low-cost, flexible, and efficient solar cells for a wide range of applications. Physical vapor deposition by co-evaporation of precursors is a method that results in very smooth and pinhole-free perovskite thin films and allows excellent control over film thickness and composition. However, for a deposition method to become industrially scalable, reproducible process control and high device yields are essential. Unfortunately, to date, the control and reproducibility of evaporating organic precursors such as methylammonium iodide (MAI) have proved extremely challenging. We show that the established method of controlling the evaporation rate of MAI with quartz microbalances (QMBs) is critically sensitive to the concentration of the impurities MAH_2PO_3 and MAH_2PO_2 that are usually present in MAI after synthesis. Therefore, controlling the deposition rate of MAI with QMBs is unreliable since the concentration of such impurities typically varies from one batch of MAI to another and even during the course of a deposition. However once reliable control of MAI deposition is achieved, we find that the presence of precursor impurities during perovskite deposition does not degrade the solar cell performance. Our results indicate that as long as precursor deposition rates are well controlled, physical vapor deposition will allow high solar cell device yields even if the purity of precursors changes from one run to another.

KEYWORDS: *solar cells, perovskites, hybrid metal-halide perovskites, co-evaporation, impurities, thermal evaporation, methylammonium iodide, residual gas analysis*

1. INTRODUCTION

Solar-to-electrical power conversion efficiencies (PCEs) of solar cells based on metal-halide perovskite semiconductors have risen from just 3.8% in 2009[1] to over 24.2%[2] in less than a decade. These perovskite semiconductors possess many properties that are ideal for energy generation, including low-energy cost for fabrication,[3] low Shockley−Read−Hall recombination rates,[4] high charge-carrier diffusion lengths and mobilities,[5] and a high absorption coefficient across much of the solar spectrum.[6] The ability to change stoichiometry to tune the band gap has recently enabled a range of planar heterojunction tandem solar cells to be realized including perovskite−silicon,[7] perovskite−CIGS,[2] and perovskite−perovskite[8] devices.

The first efficient perovskite solar cell with a planar heterojunction architecture was fabricated using the technique of vapor co-deposition in 2013.[9] In this process, organic and inorganic precursors such as methylammonium iodide (MAI) and PbI_2 are heated simultaneously in separate furnaces under vacuum. These precursors condense and react on a substrate resulting in polycrystalline perovskite film growth. Co-evaporated films grown by this method have great potential for scalable production of perovskite photovoltaics since they are uniform and free of pinholes[9,10] over a large area. The film thickness can also be controlled very accurately.[11,12] Furthermore vapor-deposited films are extremely smooth, enabling fundamental studies that require well-define interfaces and low light scattering.[13−15] Recently, it has been shown that a wide range of hybrid perovskite materials can be co-evaporated, including $FAPbI_3$,[10] $CsPbI_2Br$,[16] and $Cs_{0.5}FA_{0.4}MA_{0.1}Pb(I_{0.83}Br_{0.17})_3$,[17] where $FA=CH(NH_2)_2$ and $MA=CH_3NH_3$. Co-deposition is also particularly promising for the perovskite−perovskite tandem and multijunction solar cells as it avoids the need for solvent orthogonality required during solution processing.[18]

However, the vast majority of research to date on metal-halide perovskite solar cells has concentrated on alternative methods that require solvents such as spin-coating,[19,20] doctor-

Received: May 1, 2019
Accepted: July 17, 2019
Published: July 17, 2019

blading,[21,22] two-step deposition,[23] and solvent annealing.[24] The question arises as to why vapor co-deposition is currently underutilized. The reason in large part originates from the difficultly in reliably controlling the co-deposition process, in particular rate control of the organic precursors such as MAI.[25−27] Researchers have struggled to overcome this challenge. While some workable solutions have been reported, the underlying reasons why methylammonium iodide is so hard to evaporate controllably have not been investigated in detail.[28]

Here, we show that the reliable production of $MAPbI_3$ thin films via co-evaporation of MAI and PbI_2 is critically dependent on impurities within the organic (MAI) precursor. We focus on two impurities MAH_2PO_3 and MAH_2PO_2, as they are both commonly found in MAI powders as byproducts of MAI synthesis.[29] Their influence on the deposition of perovskite films has not been studied widely and has not been investigated for vacuum deposition at all. We find that these impurities themselves have a dramatic effect on controlling and regulating the deposition rate of MAI with quartz microbalances (QMBs). While the impurities affect the control of the deposition process, we find that the impurities have little impact on device performance. Our results help explain the difficulties researchers have faced in controlling the metal-halide perovskite co-deposition and allow us to propose more reliable deposition methodologies to overcome these problems. In addition, this study indicates that high-purity precursors are not required to vapor deposit solar cells with reasonable power conversion efficiency.

Several different strategies have been reported previously to control and monitor the evaporation rate of MAI during co-evaporation. Quartz microbalances (QMB) are commonly used to monitor the growth rate of evaporated thin films.[30] For the deposition of $MAPbI_3$, QMBs facing the MAI crucible have been employed,[9,14] as well as QMBs that are deliberately turned away from the crucible to measure the pressure in the chamber instead of the direct deposition rate.[31] A third approach utilizes a standard pressure gauge to measure the chamber pressure to control the MAI deposition.[26,32,33] The two latter approaches are often adopted after the standard QMB rate measurement could not be successfully employed to monitor and control the MAI deposition.

Many authors report difficulties determining the rate of MAI vapor deposition with standard QMBs. For example, Malinkiewicz et al.[25] commented that they were unable to calibrate the QMB sensor by measuring the thickness of the deposited MAI film. Borchert et al.[32] noted that the MAI rate can often not be properly recorded using a QMB, and Zhao et al.[33] similarly reported that they experienced difficulty calibrating and monitoring the MAI rate with a QMB and therefore decided to monitor the pressure instead. Unfortunately, the chamber pressure can depend on many factors, for example, small leaks in the chamber, residual water, and other chemicals outgassing from the chamber walls and volatile impurities in the precursors. Therefore, it is hard to draw a straightforward connection between the chamber pressure and the rate of MAI evaporation. A wide range of chamber pressures during evaporation has been reported, from around 3×10^{-3} mbar[34] to as low as 3×10^{-6} mbar,[14] with many groups reporting values in the 10^{-4}−10^{-5} mbar range.[12,26,27,32,33,35]

To study the composition of the residual gas in the vacuum chamber, we used mass spectroscopy. Only a few mass spectroscopy studies relating to MAI or $MAPbI_3$ have been reported in the literature. Most of these studies have focused on the decomposition of $MAPbI_3$,[36,37] while Bækbo et al. performed combined QMB and mass spectrometry measurements to show that MAI has a low sticking coefficient and appears to decompose into CH_3NH_2 and HI on the way from the crucible to the substrate.[38]

We used two methylammonium iodide (MAI) batches of different purities to deposit $MAPbI_3$ thin films: one high-purity MAI batch and one low-purity MAI batch, which contained impurities MAH_2PO_3 and MAH_2PO_2. Both of these impurities have a lower melting point than MAI. MAH_2PO_2 is a viscous liquid at room temperature, and MAH_2PO_3 melts around 60 °C.[29] In the vacuum chamber, MAH_2PO_3 evaporates around 55 °C, which is well below the evaporation temperature of MAI. We characterized both MAI batches with NMR measurements and infrared absorption spectroscopy. To understand the influence of the impurities on the co-evaporation of methylammonium lead triiodide ($MAPbI_3$), we monitored precursor fluxes using an in situ residual gas analysis (RGA) system and QMBs. The deposited films were also characterized using X-ray diffraction (XRD) and scanning electron microscopy (SEM). Finally, we fabricated solar cells and studied their performance. Together, these data explain the origin of the problems faced in previous studies in controlling the MAI flux and hence the $MAPbI_3$ layer quality and reproducibility. This understanding opens the way for more reliable and reproducible methods for the co-deposition of metal-halide perovskite semiconductors.

2. RESULTS AND DISCUSSION

To study the influence of impurities on the co-evaporation of methylammonium lead iodide, we synthesized and compared a high-purity MAI batch with a low-purity MAI batch. Levchuk et al.[29] previously identified two main impurities in MAI: MAH_2PO_3 and MAH_2PO_2, both of which are formed during the synthesis of MAI and derived from H_3PO_2. The source of the H_3PO_2 impurity is likely to originate from HI solutions used in the synthesis of MAI, since commercial HI is typically stabilized with H_3PO_2. Depending on how the MAI is washed and purified after the synthesis, different concentrations of MAH_2PO_3 and MAH_2PO_2 remain. First, we wanted to find out if these impurities influenced the efficiency of solar cells fabricated with our co-evaporated methylammonium lead iodide semiconductor films.

The high-purity methylammonium iodide was synthesized by mixing H_3PO_2-stabilized HI and methylamine (CH_3NH_2) in ethanol at room temperature. In contrast to the standard purification process with diethylether and ethanol only,[1,39−41] we recrystallized our material from the saturated hot solutions of MAI in ethanol, leaving all impurities in the solute. The low-purity MAI batch was purified only once with diethyl ether.

The deposition parameters for both high-purity and low-purity MAI batches were optimized separately so that efficient solar cells could be fabricated with either. It was not possible to use a QMB to monitor the high-purity MAI flux (as discussed in Section 2.4 of the Supporting Information (SI)), therefore optimization involved repeated co-evaporation of MAI and PbI_2 first varying the temperature setpoints for the MAI source each time and subsequently varying the deposition time. A standard solar cell device architecture consisting of C_{60} and Spiro-OMeTAD as contact layers was used (see Supporting Information, Section 4 for details). Stabilized efficiencies of 15.7% for the low-purity batch and 15.3% for the high-purity

DOI: 10.1021/acsami.9b07619
ACS Appl. Mater. Interfaces 2019, 11, 28851−28857

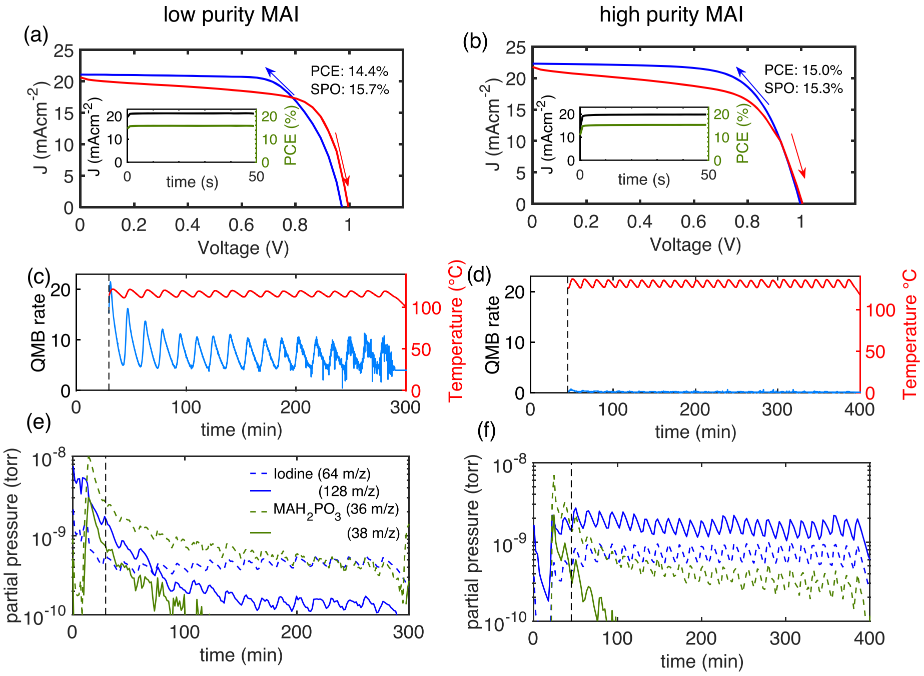

Figure 1. J−V curves of champion $MAPbI_3$ solar cells made using the low-purity MAI (a) or the high-purity MAI (b). For the low-purity MAI, the champion power conversion efficiency (PCE) was 14.4% and the stabilized power output (SPO) was 15.7%. For the high-purity MAI, the champion PCE was 15.0% and the SPO was 15.3%. During the evaporation runs, the quartz microbalance (QMB) rate and the MAI source temperature (c, d) were measured. Additionally, a residual gas analysis (RGA) system was used to track selected mass spectroscopy peaks (e, f) over the course of the respective evaporation run.

MAI were achieved. The current−voltage (J−V) curves for each of the champion cells are shown in Figure 1a,b. For both champion cells, the forward (red line) and reverse scans (blue line) are shown and a small amount of hysteresis is found probably related to an imperfect n-contact.[14] We found that while the different purity batches of MAI had different optimal source temperatures and depositions times, we were able to achieve nearly equal efficiencies using MAI precursors of different purities. This result for vapor-deposited devices is in stark contrast to the effect of the impurities MAH_2PO_3 and MAH_2PO_2 on solution-processed solar cells. Levchuk et al.[29] reported that during solution processing, these impurities in MAI can influence the $MAPbI_3$ crystallization, grain size, and solar-cell performance. They found that the solar cell solution processed from less pure MAI actually performed better than that made using highly purified MAI. This contrast highlights the different mechanisms of perovskite crystal formation between vapor- and solution-based deposition methods and their sensitivity to impurities.

While optimized solar cell performance was similar between vapor-deposited devices from different purity MAIs, we observed drastic differences between the deposition rates of MAI as observed by the QMBs. To gain a better understanding of how the impurities MAH_2PO_3 and MAH_2PO_2 influenced the observed MAI deposition rates, we performed a systematic study in which we continuously monitored three QMBs and sampled the residual gas in the deposition chamber. The three QMBs were positioned in the chamber so that one was 5 cm above each source (MAI and PbI_2) and one was at the same height as the substrate. The temperature of each source was monitored via K-type thermocouples in contact with the bases of the crucibles containing the MAI and PbI_2 precursors. Mass spectroscopy was performed continuously via a sampling RGA system connected directly to the deposition chamber at a height intermediate between the deposition sources and the sample substrate.

For these depositions, the temperature of the source containing MAI was set to a constant target temperature. The proportional-integral-derivative (PID) controller of the MAI source was intentionally detuned so that the measured temperature oscillated about the target. These oscillations were used to identify the MAI rather than PbI_2 as the source of the iodine signal in the RGA measurements. To achieve this, the PID control of the PbI_2 source temperature (based on QMB feedback) was well tuned, with the source temperature remaining constant for the duration of the deposition (as shown in the Supporting Information, Section 2.3). Therefore, we could use the temperature oscillations of the MAI source to assign unambiguously the changes seen in the RGA and QMB measurements to the MAI flux.

First, a $MAPbI_3$ film was deposited using a low-purity MAI batch. Figure 1c shows the MAI source temperature (red line) as a function of deposition time with the rate signal from the QMB closest to the MAI source overlayed (blue line). As expected, it can be seen that the small temperature oscillations associated with the detuned PID parameters lead to a large fluctuation of the QMB-observed deposition rate. The QMB signal could, in this case, have easily been used as a feedback to control the source temperature for even deposition rates. In contrast, Figure 1d shows a repeat deposition in which the low-purity MAI was replaced with the high-purity MAI. While the source temperature also oscillates, the apparent rate measured by the QMB for the high-purity MAI was very low and indistinguishable from the noise floor of the measurement. As such, QMBs clearly cannot be used as part of a control feedback loop when high-purity MAI is deposited. Thus, the QMB behaved quite differently during these two depositions and showed completely different apparent rates for the two different depositions. These results could mean that either there is actually less MAI evaporated when high-purity MAI is used or they could point to a discrepancy between the apparent rate on the QMB and the actual rate of MAI evaporation. The fact that both depositions produced $MAPbI_3$ perovskite films points to a problem with the apparent rate measured by the QMB when purified MAI is being evaporated. This explanation is confirmed by the in situ RGA data and analysis of the material deposited on the QMBs, as detailed below.

During the deposition shown in Figure 1c,d, the composition of the residual gas in the evaporation chamber was measured using the RGA. The evolution of the selected mass spectroscopy peaks over the course of the evaporations is displayed in Figure 1e,f, and the selected peaks are identified as originating from iodine (blue) and the impurity MAH_2PO_3 (green) (the assignment of these peaks is discussed later). For the case of high-purity MAI, it is immediately clear from comparison of Figure 1d,f that MAI is indeed being evaporated. The oscillation of the iodine RGA peak, which correlates with the source temperature, shows that the gaseous iodine originates from the high-purity MAI in the source. Therefore, in support of the above argument, even when the QMB is reading zero, MAI is still being evaporated, so the problem lies with the QMB not reading correctly when MAI is particularly pure, not with the actual MAI flux emitted from the furnace.

For an effective use of the residual gas analysis system to monitor the evaporation, a correct assignment of mass spectroscopy peaks to the originating material is essential. As mentioned previously, the main impurities in MAI are MAH_2PO_3 and MAH_2PO_2;[29] therefore, to identify them in the mass spectrum during co-evaporation, we performed one evaporation with only the high-purity MAI and another with only MAH_2PO_3 in the crucible. In Figure 2, we compare the MAI mass spectrum (in blue) with the MAH_2PO_3 spectrum (flipped in red below for clarity) to find unique peaks in each of the spectra. Two different detectors were installed in the mass spectrometer: the low-mass spectrum for the Faraday detector is displayed in Figure 2a, while the higher-mass spectrum obtained with a secondary electron multiplier (SEM) is shown in Figure 2b. It is evident from the comparison of the mass spectra of MAI and MAH_2PO_3 in Figure 2a that for small masses, the two spectra are very similar. Peaks at 36 and 38 m/z allow us to identify MAH_2PO_3 uniquely even in the presence of a MAI background. In the higher range of the spectrum shown in Figure 2b there are several peaks (at 64, 127, and 128 m/z), which are only present in the MAI spectrum and clearly originate from iodine present in MAI. As discussed above, the development of these unique peaks over time during the evaporation is depicted in Figure 1e,f.

We now consider the variability of impurity concentrations in MAI obtained from a range of commercial suppliers and discuss how this might affect the control and reproducibility of $MAPbI_3$ vapor co-deposition. We performed NMR measurements on seven different MAI batches (see Supporting Information, Section 1.1 for details and batch numbers), including our lab-synthesized high-purity and low-purity MAI discussed above. Figure 3a shows the proton NMR (^1H NMR) spectra for samples from each of these batches, and a summary of their NH_3 proton peak positions and the corresponding full width at half-maximum (FWHM) is displayed in Figure 3b. Levchuk et al.[29] have shown previously that the NH_3 proton

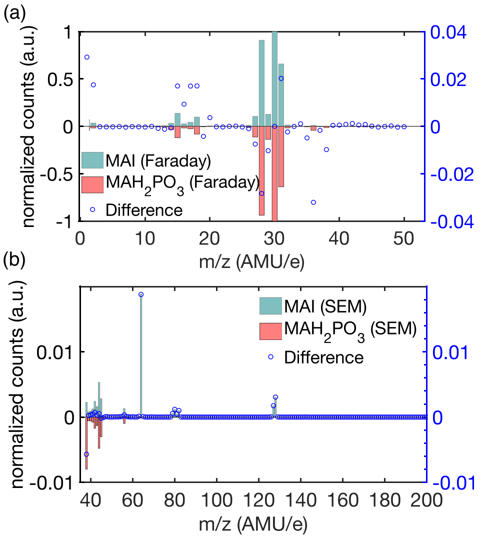

Figure 2. (a) Comparison of the mass spectra of MAI and MAH_2PO_3, both recorded with the Faraday detector of the residual gas analysis (RGA) system. (b) Comparison of the higher m/z range of the mass spectrum of MAI and MAH_2PO_3, both recorded with the secondary electron multiplier (SEM) detector of the residual gas analysis (RGA) system. The difference between the mass spectra of the two measured substances was calculated by subtracting the normalized MAH_2PO_3 value from the normalized MAI value for each m/z value and is displayed as blue circles.

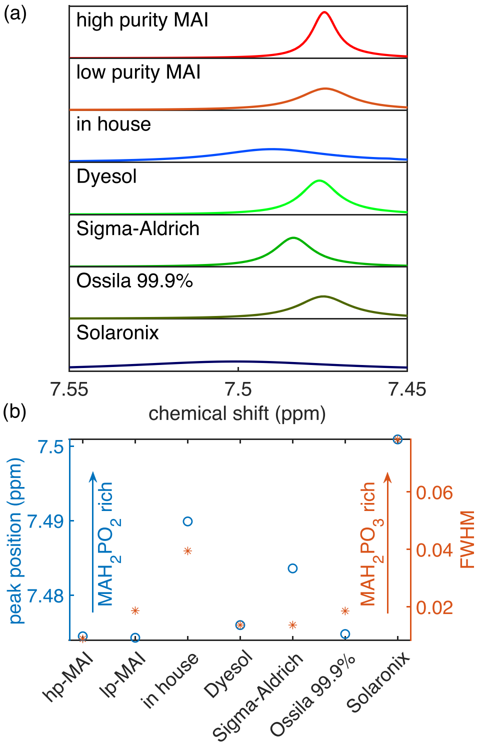

Figure 3. ^1H NMR characterization of different MAI batches. Details like batch numbers can be found in the SI. (a) NMR spectra of different MAI batches shown from 7.55 to 7.45 ppm to focus on the NH_3 proton MA peak. A clear shift of the peak maximum for different batches is observed. (b) Summary of the peak position and full width at half-maximum (FWHM) of the peak around 7.5 ppm for several MAI batches. A higher FWHM indicates that the batch is rich in MAH_2PO_3. A higher peak position indicates that it is rich in MAH_2PO_2.[29]

NMR peak shifts toward higher values when more MAH$_2$PO$_2$ impurity is present, whereas the peak broadens with increasing MAH$_2$PO$_3$ impurity concentration. We find that our high-purity MAI has the smallest FWHM and peak position of all samples, which is in agreement with Levchuk et al.'s observation. Figure 3b shows significant variations in the concentrations of MAH$_2$PO$_2$ and MAH$_2$PO$_3$ impurities in the commercially available MAI. The dependence of the apparent deposition rate on a QMB on the impurity concentration therefore explains the challenges of the control and measurement of the MAI rate during evaporation, which have been reported in the literature.

As shown in Figure 3, ^{1}H NMR measurements reveal that different commercial batches of MAI contain vastly different amounts of the two studied impurities. While the MAI batch obtained from Dyesol (now Greatcell Solar Materials) contains small amounts of MAH$_2$PO$_3$ and MAH$_2$PO$_2$, it is the purest of the commercial samples. The batch from Sigma-Aldrich contains a small amount of MAH$_2$PO$_3$ and a significant amount of MAH$_2$PO$_2$. In contrast, the MAI batch from Ossila (>99.9% purity) is very low in MAH$_2$PO$_2$ and contains some MAH$_2$PO$_3$. Finally, the batch obtained from Solaronix contains the highest concentration of both of these impurities. In comparison with these commercial samples, our lab-synthesized low-purity MAI sample is still relatively pure.

The question remains as to why the apparent rate of MAI deposition recorded by a QMB is so sensitive to small changes in the concentration of impurities in MAI. As discussed above, during evaporation runs, we observed that the reading of the quartz balance, which is mounted close to the MAI source, depends dramatically on the batch of MAI that is used (Figure 1c,d). When the low-purity MAI is used, a rate is easily detected. In contrast, when the high-purity MAI is used, the rate is low from the beginning and drops off quickly. The apparent deposition rates recorded by the QMB are vastly different even for runs that result in perovskite films of the same thickness (see Supporting Information, Section 3.2). To understand why the QMBs seem to fail in the case of MAI evaporation, we characterized the films deposited on the quartz crystals themselves. After a full co-evaporation run, we removed the QMB crystals from the chamber and performed scanning electron microscopy (SEM) and attenuated total reflectance (ATR) infrared absorption measurements to investigate any deposits on the QMBs.

Cross-sectional scanning electron micrographs of QMB sensors that monitored the MAI deposition rates from low-purity and high-purity MAIs are displayed in Figure 4a,b, respectively. The low-purity MAI formed a thick MAI layer with grains closely packed (Figure 4a) in stark contrast to the high-purity MAI, which produced a much thinner layer of platelets on the QMB crystal (Figure 4b). To confirm that the material deposited on the QMB in each case was indeed MAI, we performed ATR infrared absorption measurements on each QMB, and the resulting spectra are presented in Figure 4c. The vibrations related to the NH$_3^+$-bend appear at 2701, 1559, and 1414 cm^{-1}, while the vibrations relating to the NH$_3$CH$_3^+$-rock occur at 1244 and 905 cm^{-1}.[42] The ATR signal from the QMB sensor used during the high-purity MAI deposition is much weaker than that from the low-purity MAI. However, both do show the expected peaks for MAI, indicating that films of MAI are present in both cases, albeit of considerably different thicknesses. Thus, it appears that in both cases, MAI is deposited onto the source monitor crystal, but much less material adheres to the crystal when high-purity MAI is used compared with when low-purity MAI is used, even when the same thickness of MAPbI$_3$ is grown on the substrate.

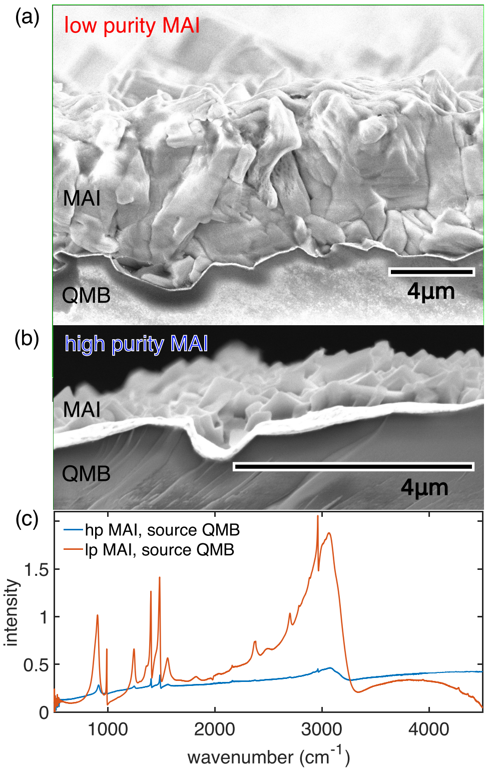

Figure 4. Cross-sectional scanning electron microscopy (SEM) images of a quartz balance used to monitor MAI evaporation during a deposition run with (a) low-purity MAI and (b) high-purity MAI. (c) Infrared spectra of those same quartz balances.

The large differences between the high- and low-purity MAIs seen in the SEM image and the IR spectrum of the source QMB are consistent with the difference in the detected MAI rate during the evaporation run displayed in Figure 1c,d. In both evaporation runs, nearly the same thickness of MAPbI$_3$ was grown on the substrate (see Supporting Information, Section 3.2). Evidently, enough MAI was deposited to achieve the desired composition as only very small lead iodide peaks appear in the XRD of the grown MAPbI$_3$ films (see Supporting Information, Section 3.1). But from the apparent rate measured by the QMB at the MAI source, one would incorrectly conclude that much less MAI was present during the evaporation with the high-purity MAI than during the run using the low-purity MAI.

Together, these measurements indicate that the sticking coefficient of pure MAI to the gold surface of the QMB is vanishingly small; however, in the presence of the impurities MAH$_2$PO$_3$ and MAH$_2$PO$_2$, MAI adheres significantly better to the gold surface. A possible mechanism for this could be that the impurities form small clusters on the gold surface, which then act as nucleation centers for MAI growth. A more detailed study would be required to test this hypothesis.

3. CONCLUSION AND OUTLOOK

To understand better the processes occurring within the vacuum chamber during the co-evaporation of MAPbI$_3$ and the influence of impurities, we utilized lab-synthesized MAI batches with two different purities and several commercial

DOI: 10.1021/acsami.9b07619
ACS Appl. Mater. Interfaces 2019, 11, 28851−28857

MAI batches for comparison. We performed depositions with different MAI batches and monitored the evaporation using quartz microbalances, a residual gas analysis system, and pressure and temperature sensors. Subsequently, we characterized the resulting films and solar cells. We found that the sticking coefficient of MAI to the gold surface of a quartz microbalance is highly sensitive to the concentration of impurities in MAI. Thus, for the same MAI flux, the thickness of the MAI film deposited onto the balance varies greatly depending on which batch is used. This explains why some groups report great difficulty with the QMB-based control of MAI deposition flux, while others were able to control the MAI rate with quartz balances.

The presence of MAH_2PO_3 and MAH_2PO_2 increases the sticking coefficient of MAI to the QMB and allows the deposition rate feedback control. This suggests that controlled concentrations of these impurities in the MAI precursor could allow reproducible QMB-controlled depositions. However, we find that the concentration of MAH_2PO_3 impurity varies during evaporation, as can be seen in Figure 1e,f. This suggests that the impurities preferentially outgas from the precursor at the beginning of the deposition, which is likely to lead to changes of the sticking coefficient of MAI to the QMB during an evaporation run. Thus, it is expected that the apparent MAI deposition rate as measured by a QMB will vary from the true rate over the course of a co-deposition.

Therefore, we find that QMBs on their own are not very reliable for monitoring MAI evaporation. Thus, additional monitoring methods should be used, for example, residual gas analysis or in situ XRD.[32] Residual gas analysis can additionally be useful to monitor deposition rates, detect possible water or halide contamination, and check for vacuum leaks. We also found that the concentration of impurities measured in the residual gas changed over the course of the deposition (see Figure 1e,f) which also complicates the QMB-based rate control even when sufficient MAI does stick to it.

In spite of difficulties in controlling the MAI deposition rates, we were able to optimize $MAPbI_3$ co-deposition for a batch of high-purity and a batch of low-purity MAI. The resulting solar cell devices had a similar performance, indicating that the impurities MAH_2PO_3 and MAH_2PO_2 have little effect on the function of co-evaporated $MAPbI_3$. These results are very promising, as they show that we have not yet reached the full potential of vapor-deposited solar cell performance owing to a lack of reliable process control. Once an accurate rate control of all precursors is achieved, rapid growth optimization will be achieved, which should lead to significant improvement in the performance and reproducibility of vapor-deposited metal-halide solar cells. An overall understanding of the source of growth irreproducibility and developing better deposition control methods will enable vapor co-deposition to become the method of choice for upscaling solar cell production to an industrially relevant scale.

■ ASSOCIATED CONTENT

Supporting Information

The Supporting Information is available free of charge on the ACS Publications website at DOI: 10.1021/acsami.9b07619.

Further information about the precursors, deposition monitoring system, thin film, and device characterization (PDF)

■ AUTHOR INFORMATION

Corresponding Author

*E-mail: michael.johnston@physics.ox.ac.uk.

ORCID

Ievgen Levchuk: 0000-0003-0644-2283
Henry J. Snaith: 0000-0001-8511-790X
Laura M. Herz: 0000-0001-9621-334X
Michael B. Johnston: 0000-0002-0301-8033

Notes

The authors declare no competing financial interest.

■ ACKNOWLEDGMENTS

The authors gratefully acknowledge the financial support from the Engineering and Physical Sciences Research Council (U.K.) (EPSRC) via grants EP/P006329/1 and EP/P033229/1. J.B. thanks the EPSRC for funding via the Centre for Doctoral Training in New and Sustainable Photovoltaics. C.J.B. acknowledges funding through the state of Bavaria by the project "Solar goes Hybrid".

■ REFERENCES

(1) Kojima, A.; Teshima, K.; Shirai, Y.; Miyasaka, T. Organometal Halide Perovskites as Visible-Light Sensitizers for Photovoltaic Cells. *J. Am. Chem. Soc.* **2009**, *131*, 6050−6051.

(2) Green, M. A.; Dunlop, E. D.; Levi, D. H.; Hohl-Ebinger, J.; Yoshita, M.; Ho-Baillie, A. W. Y. Solar Cell Efficiency Tables (Version 54). *Prog. Photovoltaics* **2019**, *27*, 565−575.

(3) Brittman, S.; Adhyaksa, G. W. P.; Garnett, E. C. The Expanding World of Hybrid Perovskites: Materials Properties and Emerging Applications. *MRS Commun.* **2015**, *5*, 7−26.

(4) Herz, L. M. Charge Carrier Dynamics in Organic-Inorganic Metal Halide Perovskites. *Annu. Rev. Phys. Chem.* **2016**, *67*, 65−89.

(5) Wehrenfennig, C.; Eperon, G. E.; Johnston, M. B.; Snaith, H. J.; Herz, L. M.; Michael, B. High Charge Carrier Mobilities and Lifetimes in Organolead Trihalide Perovskites. *Adv. Mater.* **2013**, *26*, 1584−1589.

(6) Xing, G.; Mathews, N.; Sun, S.; Lim, S. S.; Lam, Y. M.; Grätzel, M.; Mhaisalkar, S.; Sum, T. C. Long-Range Balanced Electron- and Hole-Transport Lengths in Organic-Inorganic $CH_3NH_3PbI_3$. *Science* **2013**, *342*, 344−347.

(7) McMeekin, D. P.; Sadoughi, G.; Rehman, W.; Eperon, G. E.; Saliba, M.; Hörantner, M. T.; Haghighirad, A.; Sakai, N.; Korte, L.; Rech, B.; Johnston, M. B.; Herz, L. M.; Snaith, H. J. A Mixed-Cation Lead Mixed-Halide Perovskite Absorber for Tandem Solar Cells. *Science* **2016**, *351*, 151−155.

(8) Eperon, G. E.; Leijtens, T.; Bush, K. A.; Prasanna, R.; Green, T.; Wang, J. T.; McMeekin, D. P.; Volonakis, G.; Milot, R. L.; May, R.; Palmstrom, A.; Slotcavage, D. J.; Belisle, R. A.; Patel, J. B.; Parrott, E. S.; Sutton, R. J.; Ma, W.; Moghadam, F.; Conings, B.; Babayigit, A.; Boyen, H.-g.; Bent, S.; Mcgehee, M. D.; Snaith, H. J.; et al. Perovskite-Perovskite Tandem Photovoltaics with Optimized Band Gaps. *Science* **2016**, *354*, 861−866.

(9) Liu, M.; Johnston, M. B.; Snaith, H. J. Efficient Planar Heterojunction Perovskite Solar Cells by Vapour Deposition. *Nature* **2013**, *501*, 395−398.

(10) Borchert, J.; Milot, R. L.; Patel, J. B.; Davies, C. L.; Wright, A. D.; Martínez Maestro, L.; Snaith, H. J.; Herz, L. M.; Johnston, M. B. Large-Area, Highly Uniform Evaporated Formamidinium Lead Triiodide Thin Films for Solar Cells. *ACS Energy Lett.* **2017**, *2*, 2799−2804.

(11) Longo, G.; Momblona, C.; La-Placa, M.-G.; Gil-Escrig, L.; Sessolo, M.; Bolink, H. J. Fully Vacuum-Processed Wide Band Gap Mixed-Halide Perovskite Solar Cells. *ACS Energy Lett.* **2018**, *3*, 214−219.

(12) Erdenebileg, E.; Scholz, L. E.; Hofacker, A.; Koerner, C.; Leo, K. Very Small Inverted Hysteresis in Vacuum-Deposited Mixed

Organic-Inorganic Hybrid Perovskite Solar Cells. *Energy Technol.* **2017**, *5*, 1606−1611.

(13) Davies, C. L.; Borchert, J.; Xia, C. Q.; Milot, R. L.; Kraus, H.; Johnston, M. B.; Herz, L. M. Impact of the Organic Cation on the Optoelectronic Properties of Formamidinium Lead Triiodide. *J. Phys. Chem. Lett.* **2018**, *9*, 4502−4511.

(14) Patel, J. B.; Wong-Leung, J.; Van Reenen, S.; Sakai, N.; Wang, J. T. W.; Parrott, E. S.; Liu, M.; Snaith, H. J.; Herz, L. M.; Johnston, M. B. Influence of Interface Morphology on Hysteresis in Vapor-Deposited Perovskite Solar Cells. *Adv. Electron. Mater.* **2016**, *3*, No. 1600470.

(15) Patel, J. B.; Milot, R. L.; Wright, A. D.; Herz, L. M.; Johnston, M. B. Formation Dynamics of $CH_3NH_3PbI_3$ Perovskite Following Two-Step Layer Deposition. *J. Phys. Chem. Lett.* **2016**, *7*, 96−102.

(16) Park, C.-G.; Choi, W.-G.; Na, S.; Moon, T. All-Inorganic Perovskite $CsPbI_2Br$ Through Co-evaporation for Planar Heterojunction Solar Cells. *Electron. Mater. Lett.* **2019**, *15*, 56−60.

(17) Gil-Escrig, L.; Momblona, C.; La-Placa, M. G.; Boix, P. P.; Sessolo, M.; Bolink, H. J. Vacuum Deposited Triple-Cation Mixed-Halide Perovskite Solar Cells. *Adv. Energy Mater.* **2018**, *8*, No. 1703506.

(18) Jiang, F.; Liu, T.; Luo, B.; Tong, J.; Qin, F.; Xiong, S.; Li, Z.; Zhou, Y. A Two-Terminal Perovskite/Perovskite Tandem Solar Cell. *J. Mater. Chem. A* **2016**, *4*, 1208−1213.

(19) Im, J.-H.; Lee, C.-R.; Lee, J.-W.; Park, S.-W.; Park, N.-G. 6.5% Efficient Perovskite Quantum-Dot-Sensitized Solar Cell. *Nanoscale* **2011**, *3*, 4088−4093.

(20) Kim, H.-S.; Lee, C.-R.; Im, J.-H.; Lee, K.-B.; Moehl, T.; Marchioro, A.; Moon, S.-J.; Humphry-Baker, R.; Yum, J.-H.; Moser, J. E.; Grätzel, M.; Park, N.-G. Lead Iodide Perovskite Sensitized All-Solid-State Submicron Thin Film Mesoscopic Solar Cell with Efficiency Exceeding 9%. *Sci. Rep.* **2012**, *2*, No. 591.

(21) Back, H.; Kim, J.; Kim, G.; Kyun Kim, T.; Kang, H.; Kong, J.; Ho Lee, S.; Lee, K. Interfacial Modification of Hole Transport Layers for Efficient Large-Area Perovskite Solar Cells Achieved via Blade-Coating. *Sol. Energy Mater. Sol. Cells* **2016**, *144*, 309−315.

(22) Deng, Y.; Peng, E.; Shao, Y.; Xiao, Z.; Dong, Q.; Huang, J. Scalable Fabrication of Efficient Organolead Trihalide Perovskite Solar Cells with Doctor-Bladed Active Layers. *Energy Environ. Sci.* **2015**, *8*, 1544−1550.

(23) Burschka, J.; Pellet, N.; Moon, S.-J.; Humphry-Baker, R.; Gao, P.; Nazeeruddin, M. K.; Grätzel, M. Sequential Deposition as a Route to High-Performance Perovskite-Sensitized Solar Cells. *Nature* **2013**, *499*, 316−319.

(24) Chen, Q.; Zhou, H.; Hong, Z.; Luo, S.; Duan, H.-S.; Wang, H.-H.; Liu, Y.; Li, G.; Yang, Y. Planar Heterojunction Perovskite Solar Cells via Vapor Assisted Solution Process. *J. Am. Chem. Soc.* **2014**, *136*, 622−625.

(25) Malinkiewicz, O.; Yella, A.; Lee, Y. H.; Espallargas, G. M.; Graetzel, M.; Nazeeruddin, M. K.; Bolink, H. J. Perovskite Solar Cells Employing Organic Charge-Transport Layers. *Nat. Photonics* **2013**, *8*, 128−132.

(26) Polander, L. E.; Pahner, P.; Schwarze, M.; Saalfrank, M.; Koerner, C.; Leo, K. Hole-Transport Material Variation in Fully Vacuum Deposited Perovskite Solar Cells. *APL Mater.* **2014**, *2*, No. 081503.

(27) Pistor, P.; Borchert, J.; Fränzel, W.; Csuk, R.; Scheer, R. Monitoring the Phase Formation of Coevaporated Lead Halide Perovskite Thin Films by in Situ X-ray Diffraction. *J. Phys. Chem. Lett.* **2014**, *5*, 3308−3312.

(28) Ávila, J.; Momblona, C.; Boix, P. P.; Sessolo, M.; Bolink, H. J. Vapor-Deposited Perovskites: The Route to High-Performance Solar Cell Production? *Joule* **2017**, *1*, 431−442.

(29) Levchuk, I.; Hou, Y.; Gruber, M.; Brandl, M.; Herre, P.; Tang, X.; Hoegl, F.; Batentschuk, M.; Osvet, A.; Hock, R.; Peukert, W.; Tykwinski, R. R.; Brabec, C. J. Deciphering the Role of Impurities in Methylammonium Iodide and Their Impact on the Performance of Perovskite Solar Cells. *Adv. Mater. Interfaces* **2016**, No. 1600593.

(30) Sauerbrey, G. Verwendung von Schwingquarzen zur Wägung dünner Schichten und zur Mikrowägung. *Z. Physik* **1959**, *155*, 206−222.

(31) Ono, L. K.; Wang, S.; Kato, Y.; Raga, S. R.; Qi, Y. Fabrication of Semi-Transparent Perovskite Films with Centimeter-Scale Superior Uniformity by the Hybrid Deposition Method. *Energy Environ. Sci.* **2014**, *7*, 3989−3993.

(32) Borchert, J.; Boht, H.; Fränzel, W.; Csuk, R.; Scheer, R.; Pistor, P. Structural Investigation of Co-Evaporated Methyl Ammonium Lead Halide Perovskite Films During Growth and Thermal Decomposition Using Different PbX_2 (X = I, Cl) Precursors. *J. Mater. Chem. A* **2015**, *3*, 19842−19849.

(33) Zhao, D.; Ke, W.; Grice, C. R.; Cimaroli, A. J.; Tan, X.; Yang, M.; Collins, R. W.; Zhang, H.; Zhu, K.; Yan, Y. Annealing-Free Efficient Vacuum-Deposited Planar Perovskite Solar Cells with Evaporated Fullerenes as Electron-Selective Layers. *Nano Energy* **2016**, *19*, 88−97.

(34) Ono, L. K.; Leyden, M. R.; Wang, S.; Qi, Y. Organometal Halide Perovskite Thin Films and Solar Cells by Vapor Deposition. *J. Mater. Chem. A* **2015**, 1−21.

(35) Teuscher, J.; Ulianov, A.; Müntener, O.; Grätzel, M.; Tétreault, N. Control and Study of the Stoichiometry in Evaporated Perovskite Solar Cells. *ChemSusChem* **2015**, *8*, 3847−3852.

(36) Nenon, D. P.; Christians, J. A.; Wheeler, L. M.; Blackburn, J. L.; Sanehira, E. M.; Dou, B.; Olsen, M. L.; Zhu, K.; Berry, J. J.; Luther, J. M. Structural and Chemical Evolution of Methylammonium Lead Halide Perovskites During Thermal Processing from Solution. *Energy Environ. Sci.* **2016**, 2072−2082.

(37) Juarez-Perez, E. J.; Hawash, Z.; Raga, S. R.; Ono, L. K.; Qi, Y. Thermal Degradation of $CH_3NH_3PbI_3$ Perovskite into NH_3 and CH_3I Gases Observed by Coupled Thermogravimetry-Mass Spectrometry Analysis. *Energy Environ. Sci.* **2016**, *9*, 3406−3410.

(38) Bækbo, M. J.; Hansen, O.; Chorkendorff, I.; Vesborg, P. C. K. Deposition of Methylammonium Iodide via Evaporation-Combined Kinetic and Mass Spectrometric Study. *RSC Adv.* **2018**, *8*, 29899−29908.

(39) Lee, M. M.; Teuscher, J.; Miyasaka, T.; Murakami, T. N.; Snaith, H. J. Efficient Hybrid Solar Cells Based on Meso-Superstructured Organometal Halide Perovskites. *Science* **2012**, *338*, 643−637.

(40) Zhang, W.; Pathak, S.; Sakai, N.; Stergiopoulos, T.; Nayak, P. K.; Noel, N. K.; Haghighirad, A. A.; Burlakov, V. M.; DeQuilettes, D. W.; Sadhanala, A.; Li, W.; Wang, L.; Ginger, D. S.; Friend, R. H.; Snaith, H. J. Enhanced Optoelectronic Quality of Perovskite Thin Films with Hypophosphorous Acid for Planar Heterojunction Solar Cells. *Nat. Commun.* **2015**, *6*, No. 10030.

(41) Yan, K.; Long, M.; Zhang, T.; Wei, Z.; Chen, H.; Yang, S.; Xu, J. Hybrid Halide Perovskite Solar Cell Precursors: Colloidal Chemistry and Coordination Engineering behind Device Processing for High Efficiency. *J. Am. Chem. Soc.* **2015**, *137*, 4460−4468.

(42) Cabana, A.; Sandordy, C. The Infrared Spectra of Solid Methylammonium Halides. *Spectrochim. Acta* **1962**, *18*, 843−861.

DOI: 10.1021/acsami.9b07619
ACS Appl. Mater. Interfaces 2019, 11, 28851−28857